

Arizona Random Forest Flood Mapping

Travis Zalesky¹

¹University of Arizona,

Corresponding author: Travis Zalesky, travisz@arizona.edu

4 **Abstract**

5 Federal Emergency Management Administration 100-year flood risk maps are ex-
 6 panded across the state of Arizona using a random forest, machine learning classifi-
 7 cation utilizing eight topographic explanatory variables.

8 **Plain Language Summary**

9 Flood mapping across Arizona.

10 **1 Background**

11 A critical component of the Arizona Department of Water Resources (ADWR) Tri-
 12 University Recharge Project (TURP, a.k.a ATUR) is a state wide assessment of
 13 flooding potential. Initial efforts focused on a traditional suitability analysis ap-
 14 proach, using the analytical hierarchy process (AHP) for multi-criterion decision
 15 making, largely based on the work by Aloui et al. (2024). These methods saw initial
 16 success, and are continuing to be developed and refined. However, it became appar-
 17 ent that there were a number of shortcomings inherent in this analysis which are not
 18 easily addressed.

19 Firstly, the results of such an analysis are intrinsically linked to the data layers used,
 20 and the weighting schema determined by the AHP. As additional data sets became
 21 available, and alternate weighting schemas were tested we generated multiple ver-
 22 sions of mapped flood potential which did not necessarily agree with each other. In
 23 the absence of high quality ground-truthed data it was difficult to validate these
 24 results and it was not clear to the project team which version was the best. This
 25 underscores the need for expert involvement at every stage in these AHP based
 26 analysis. While there is a wealth of hydrological expertise within the larger ATUR
 27 project, method development and implementation has largely been conducted by
 28 a GIS technician with marginal hydrologic knowledge, and it has been difficult to
 29 foster sustained buy-in from team members on this portion of the project.

30 Furthermore, it was extremely difficult to develop a single generalized model that
 31 would be effective across the whole state. Because of the wide array of ecological
 32 and geologic conditions that are present across the state variables that are important
 33 for flood risk in one region may not apply in other regions. Lastly, even if these tech-
 34 nical issues could be overcome, there was still gaps in the input data layers, resulting
 35 in unclassified regions.

36 While the traditional suitability analysis methods of assessing flood potential is still
 37 valuable to the project, and will be retained and developed further, the reality of
 38 these challenges lead us to reevaluate our overall approach and consider alternate
 39 methods. Work by Mudashiru et al. (2021) summarized the various methods used
 40 by other researchers in this field, which includes AHP based methods as well as
 41 physical modeling and machine learning applications. The machine learning methods
 42 utilized by Tehrany et al. (2019) appeared to be particularly relevant and applica-
 43 ble. In particular, their use of topographic data **only** was particularly intriguing.
 44 These data sets are fully calculable from a digital elevation model (DEM), which are
 45 readily available, easily accessible, and have full coverage over the study area. These
 46 findings lead to a renewed initiative to apply a machine learning based method
 47 towards the objective of a state wide flooding potential map.

48 **2 Data & Methods**

49 **2.1 Topography Data**

50 All explanatory variables for the model were derived from the NASA Shuttle Radar
 51 Topography Mission (SRTM) 30-m DEM. Slope, aspect, curvature, stream power
 52 index (SPI), topographic wetness index (TWI), and sediment transport index (STI)
 53 were all calculated in ArcGIS Pro (3.4.3). Slope, aspect and curvature were calcu-

54 lated using the Surface Parameters tool (Spatial Analyst). SPI, TWI, and STI were
 55 calculated as per Tehrany et al. (2019) using the Raster Calculator according to
 56 Equations 1-3

$$SPI = A_s * \tan() \quad (1)$$

$$TWI = \ln(A_s / \tan()) \quad (2)$$

$$STI = (A_s / 22.13)^{0.6} * (\sin() / 0.0896)^{1.3} \quad (3)$$

57 where A_s is catchment area (m) and β is slope (radians).

58 Similarly, Topographic Roughness Index (TRI) was calculated as per Tehrany et al.
 59 (2019) using a custom R (4.4.1) function with the package terra (1.7-78) according
 60 to Equation 4

$$TRI = \left[\sum (\chi_{ij} - \chi_{00})^2 \right]^{0.5} \quad (4)$$

61 where χ_{ij} is the elevation at coordinates (i, j) and χ_{00} is the elevation at coordinates
 62 (0, 0) for a 3x3 focal neighborhood. The code used to calculate TRI is available on
 63 [GitHub](#).

64 2.2 Flooding Data

65 Flood data used for training the model was obtained from the Federal Emergency
 66 Management Administration (FEMA) National Flood Hazards Layer, which pro-
 67 vides 100-year flood maps for many areas of the US. The data was manually down-
 68 loaded for each county in AZ from the FEMA [data viewer](#) (accessed 3/15/2025).
 69 Data layers were merged in ArcGIS Pro (3.4.3), and the vector data was converted
 70 to a raster with a 10 m resolution. Additionally, the FEMA data was reclassified
 71 to a binary output, either flooded or not flooded (during a 100-year flood event),
 72 eliminating details such as survey methods and flow depth.

73 2.3 Variable Collinearity

74 The machine learning model was performed in Google Earth Engine (GEE). The
 75 SRTM elevation data was access and clipped to the study area natively through
 76 GEE servers, all other data layers, including the study area shapefile, were uploaded
 77 as an asset to GEE prior to model implementation.

78 Prior to modeling, the collinearity of the explanatory variables was explored using a
 79 series of pair-wise linear regression plots shown in Figures A1-A36. For collinearity
 80 analysis 5,000 points (the maximum number of points which can be plotted in GEE)
 81 were randomly sampled across the study area . The collinearity of each pair-wise
 82 regression is summarized visually in Figure 1 using the R-squared statistic of each
 83 comparison. While some relationships, e.g. slope and TWI, share a complex relation-
 84 ship that is not captured by a linear regression, the R-squared statistic is a simple
 85 indicator of collinearity which is readily understood. Although a formal variance
 86 inflation factor (VIF) analysis was not performed, efforts were made to limit model
 87 complexity by manually testing variable combinations, especially those that showed
 88 high degrees of collinearity, and at equivalent model accuracy, simpler models were
 89 preferred.

	Flood	Elevation	Slope	Aspect	Curvature	SPI	TWI	TRI
Elevation	3.70E-02							
Slope	2.00E-02	4.40E-02						
Aspect	8.83E-04	6.13E-06	1.47E-03					
Curvature	1.66E-06	3.82E-04	1.10E-02	2.28E-03				
SPI	1.67E-03	4.65E-05	7.41E-03	1.11E-05	3.41E-03			
TWI	1.10E-02	2.43E-03	1.51E-03	3.98E-03	1.82E-01	8.79E-03		
TRI	1.80E-02	3.80E-02	9.55E-01	1.31E-03	1.40E-02	9.78E-03	9.49E-04	
STI	1.91E-06	1.36E-05	1.70E-02	7.13E-05	7.81E-03	8.07E-01	8.07E-03	2.70E-02

Figure 1: Color coded R-squared statistic for each pair-wise linear regression (green = high, red = low), representing the collinearity of each variable used for modeling.

2.4 Initial Model Testing and Development

Many models were iteratively explored using several machine learning algorithms, various combinations of explanatory variables, and many hyperparameterization values. For all initial model trials the study area was reduced to the San Pedro watershed, a well characterized watershed with approx. 66% FEMA flood map coverage (visual estimate). A 70:30::training:testing data structure was adopted, and while a range of sampled points were tested, this ratio was maintained throughout. Model performance was primarily assessed through an overall accuracy score, with confusion matrix analysis performed for highly accurate models.

Tested models included Classification and Regression Tree (CART, a.k.a Decision Tree), Random Forest (RF), and Support Vector Machine (SVM). Generally, CART classification produced very noisy results which tended to overestimate flood waters, and averaged around 79.5% accuracy (data not shown). SVM classification was too computationally demanding, even within the smaller study area of the San Pedro, and given the generous cloud computing resources of GEE. As a consequence SVM classification can not be evaluated, other than to say that it is inefficient and implementation is impractical. RF classification proved to be the most promising method of classification, and the most effort was spent on developing that model.

2.4.1 Random Forest Model Development

Over 400 RF models were tested for the San Pedro watershed. Model optimization parameters tested included the number of trees, the number of sampling points (from 20,000 up to 60,000), and combinations of explanatory variables. Many RF models were tested simultaneously with between 5 to 100 trees using a custom GEE function modified from Nicolau et al. (2023). The referenced accuracy scores for preliminary models refers to the most accurate model, using the fewest number of trees. Tested RF models ranged from 73.9% to 87.4% (Table 1). The most accurate model tested used 35,000 sampling points, consisting of 30,000 dry land points (not flooded) and 5,000 flooded points and with all explanatory variables except for TRI, achieving a peak overall accuracy of 87.4% at 70 trees.

Table 1: Random Forest algorithm optimization and accuracy. All recorded sampling points grouped together before being partitioned into a 70:30::training:testing structure.

Variables	Sampling Points (dry land, flooded)	Trees	Accuracy (%)
All	15000, 5000	50	79.2
All	20000, 5000	85	82

Table 2: The confusion matrix for the most accurate random forest classifier of the San Pedro watershed, including overall, producer's and consumer's accuracy.

Predicted	Actual		0.881	Consumer's
	Dry	Flood		
Dry	8882	1199	0.881	Consumer's
Flood	126	275		
Producer's	0.986		0.874	Overall

Variables	Sampling Points (dry land, flooded)	Trees	Accuracy (%)
All	20000, 10000	85	73.9
All	25000, 5000	50	84.8
All	30000, 5000	45	87
All	30000, 10000	80	78.9
All	40000, 10000	50	82.1
All	50000, 10000		Error
No TRI	25000, 5000	90	84.9
No slope	25000, 5000	70	84.8
No TRI	30000, 5000	70	87.4
No TRI or STI	30000, 5000	40	87.2
No STI	30000, 5000	??	87.1
No elev	30000, 5000	90	86.3
No slope	30000, 5000	80	87.2
No aspec	30000, 5000	60	87
No curve	30000, 5000	40	87.1
No SPI	30000, 5000	70	87.1
No TWI	30000, 5000	40	87.1

Confusion matrix analysis for this model showed much higher producers accuracy (98.6%) compared to consumers accuracy (88.1%; Table 2). While these results are still satisfactory, they reveal that the model is generally favoring dry land classification over flooded. This can easily be explained by the relative abundance of dry land pixels vs. flooded pixels, both in the sampling points and within the FEMA training image as a whole. Qualitatively, the model appeared to be overfit to stream channels (high SPI and STI), and while many of the larger flood plains were effectively captured, flooded features generally appeared too narrow, especially along smaller tributaries. Additionally, the results were quite noisy, with noticeable speckling in both the dry and flooded regions (Figure 2 B).

2.4.2 Post-Processing

To clean up the RF classification, and further increase its overall accuracy, I post-processed the classification image using a two step process. Firstly, pixel “connectedness” was measured (D8), with pixel groups of 20 or fewer pixels reclassified to 0 (dry land). This process was very effective at removing the speckling, where small pockets were being incorrectly classified as flooded. Secondly, all remaining flooded areas were dilated using a focal maximum function using a square kernel with a 90 m radius (7x7 pixel neighborhood). This both removed noise within the flooded areas, and widened the flood zone along long, thin features, such as tributaries (Fig-

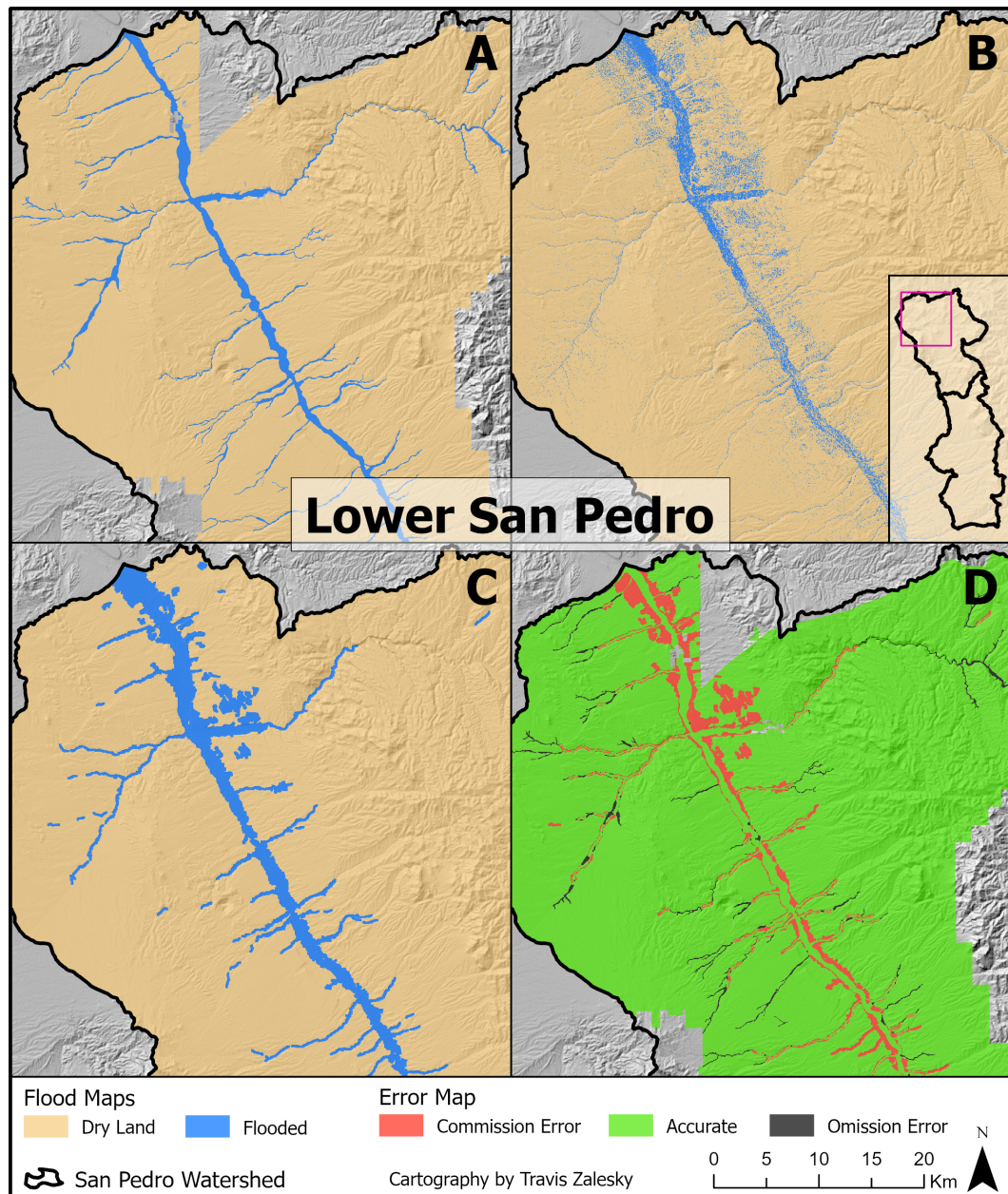


Figure 2: Side-by-side comparison of FEMA 100-year flood maps (A), raw random forest classification (B), post-processed random forest classification (C), and classification errors of the post-processed classification (D) for the lower San Pedro watershed.

Table 3: The confusion matrix for the post-processed random forest classifier of the San Pedro watershed, including overall, producer's and consumer's accuracy.

Predicted	Actual		Consumer's	Overall
	Dry	Flood		
Dry	8761	754	0.973	
Flood	247	720		
Producer's	0.973		0.905	Overall

Table 4: The confusion matrix for the random forest classifier of the full ATUR study area, encompassing Arizona, including overall, producer's and consumer's accuracy.

Predicted	Actual		Consumer's	Overall
	Dry	Flood		
Dry	8852	1249	0.987	
Flood	121	242		
Producer's	0.987		0.869	Overall

ure 2 C). This process did increase the overall rate of commission errors (incorrectly classifying as flooded), particularly along the banks of major floodplains, however the decreased rate of omission errors (incorrectly classifying as not flooded) more than made up for this fact, and the overall accuracy increased to 90.5% (Figure 2 D; Table 3)

2.5 Scaling up

The chosen RF classification, with post-processing was then applied to the larger ATUR study area, encompassing AZ. The same number of sample points were used and they retained the same structure (i.e. dry, flooded, and training, testing), however the sample locations were adjusted to the larger study area. The overall accuracy of the raw model output measured 86.9% (#tbl-confusion3). Unfortunately, while the dilated model was successful and has been exported from GEE, the associated accuracy assessment timed out and will have to be completed as a secondary process either withing GEE or using external software. Final accuracy assessment of the dilated model is pending.

2.6 Combining Data Sets

Using the newly developed RF classification the FEMA flood map can be augmented and extended to continuous coverage of Arizona. Assuming that the FEMA data is the more accurate dataset, it is given priority. The RF data is then used where no FEMA data exists. Additionally, classification error maps are generated as the difference between the RF classification, and the FEMA classification. These data layers are available for use by the ATUR project participants in the associated ArcGIS online (AGOL) group.

3 Conclusion

A state-wide binary classification of flooded areas, given a 100-year flood event, has be generated through the combination of high quality FEMA data, and a ML RF

classification algorithm used to complement and extend the FEMA data. The classification was carried out using 7 topographic explanatory variables, achieving an overall accuracy of at least 86.9% (final accuracy assessment pending). These newly developed data layers are appropriate for use within the ATUR project, for such analysis as Flood-MAR. Furthermore, I am unaware of any other continuous flood map for the state of AZ, making this work novel and potentially useful outside of the ATUR group. While improvements could certainly be made to this model, accuracy approaching (or exceeding) 90% are laudable, and these datasets may warrant external publication, pending approval.

Full project code available on [GEE](#).

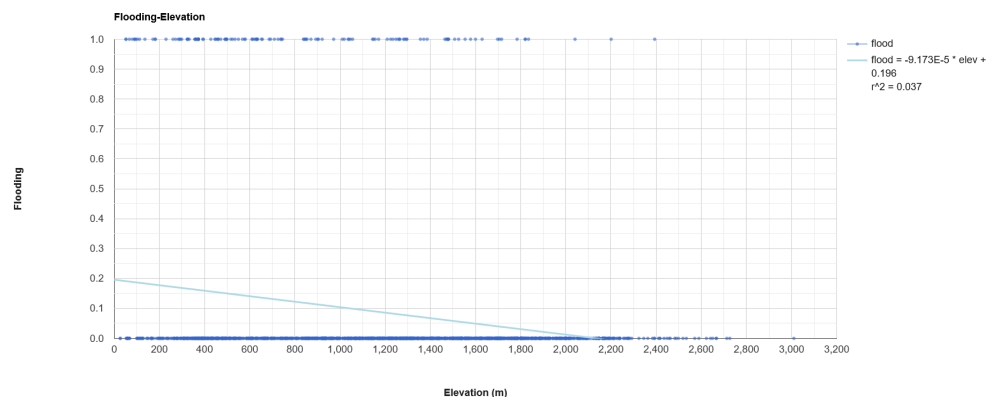
References

- Aloui, S., Zghibi, A., Mazzoni, A., Elomri, A., & Al-Ansari, T. (2024). *Identifying suitable zones for integrated aquifer recharge and flood control in arid qatar using GIS-based multi-criteria decision-making*. 25, 101137. <https://doi.org/10.1016/j.gsd.2024.101137>
- Mudashiru, R. B., Sabtu, N., Abustan, I., & Balogun, W. (2021). Flood hazard mapping methods: A review. *Journal of Hydrology*, 603, 126846. <https://doi.org/10.1016/j.jhydrol.2021.126846>
- Nicolau, A. P., Dyson, K., Saah, D., & Clinton, N. (2023). Chapter F2.2: Accuracy assessment: Quantifying classification quality. In J. A. Cardille, N. Clinton, M. A. Crowley, & D. Saah (Eds.), *Cloud-based remote sensing with google earth engine: Fundamentals and applications* (1st ed.). Springer Cham. https://docs.google.com/document/d/1UCB900oCdJERca-2WUeD1Cu52MjPKJxETJ_jJcLM0bM/edit?tab=t.0
- Tehrany, M. S., Jones, S., & Shabani, F. (2019). Identifying the essential flood conditioning factors for flood prone area mapping using machine learning techniques. *CATENA*, 175, 174–192. <https://doi.org/10.1016/j.catena.2018.12.011>

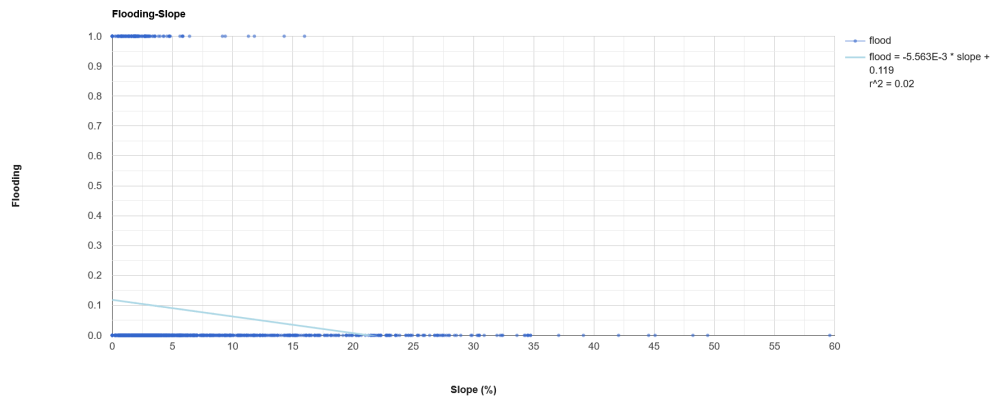
4 Appendix

Code used to render these plots, as well as interactive versions of these plots are available on [GEE](#).

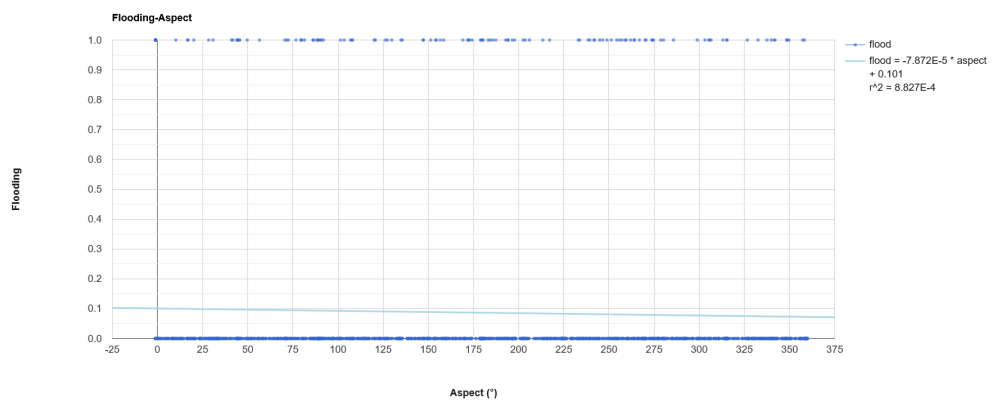
Flooding



A 1: Linear regression analysis of flood risk (binary) and elevation (m) for 5,000 randomly sampled points across the full study area, encompassing Arizona.

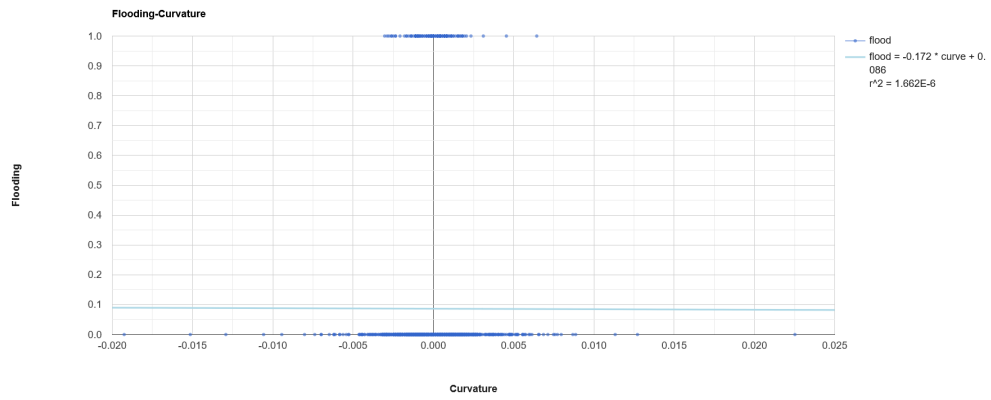


A 2: Linear regression analysis of flood risk (binary) and slope ($^{\circ}$) for 5,000 randomly sampled points across the full study area, encompassing Arizona.

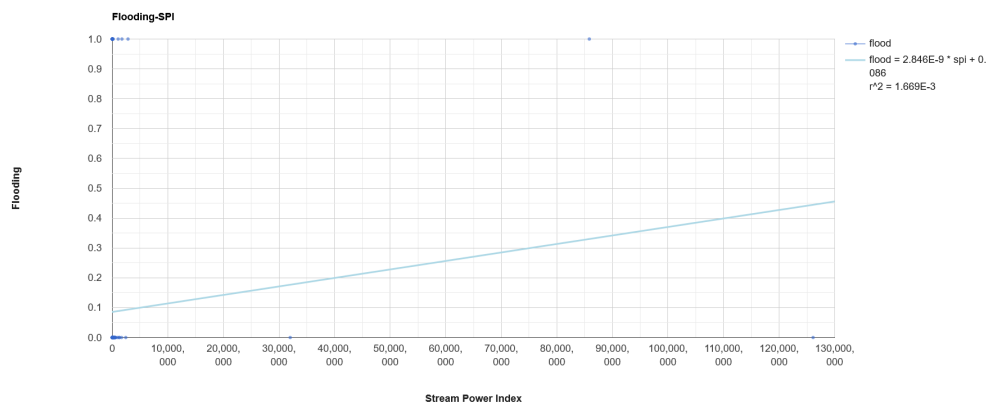


A 3: Linear regression analysis of flood risk (binary) and aspect ($^{\circ}$) for 5,000 randomly sampled points across the full study area, encompassing Arizona.

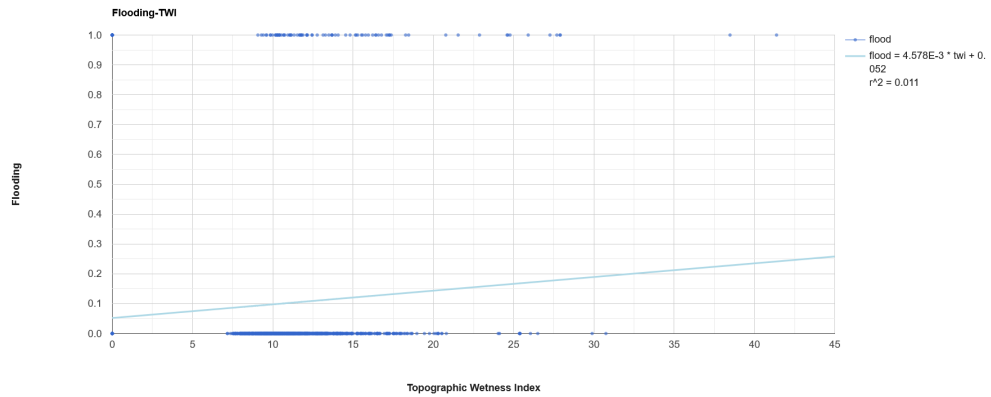
195 **Elevation**
 196 **Slope**
 197 **Aspect**
 198 **Curvature**
 199 **Stream Power Index**
 200 **Topographic Wetness Index**
 201 **Topographic Roughness Index**



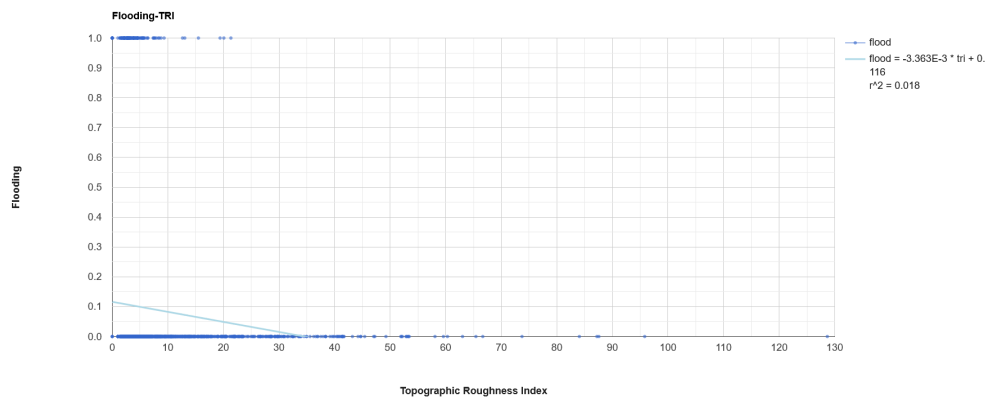
A 4: Linear regression analysis of flood risk (binary) and curvature for 5,000 randomly sampled points across the full study area, encompassing Arizona.



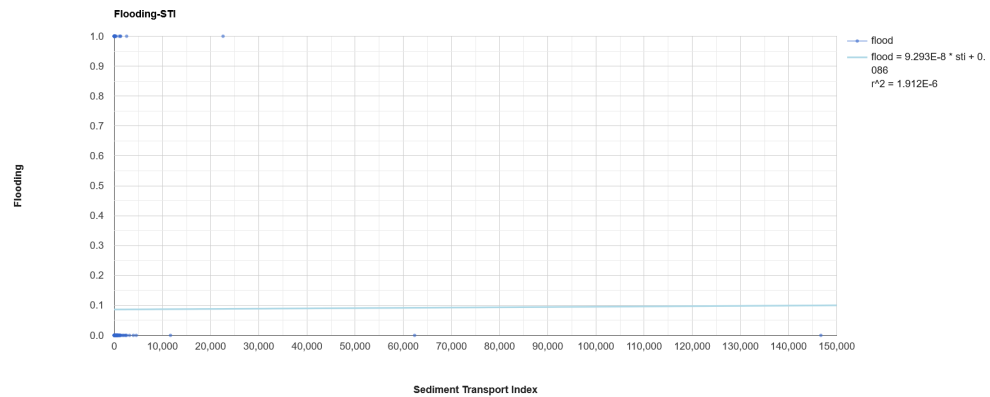
A 5: Linear regression analysis of flood risk (binary) and stream power index (SPI) for 5,000 randomly sampled points across the full study area, encompassing Arizona.



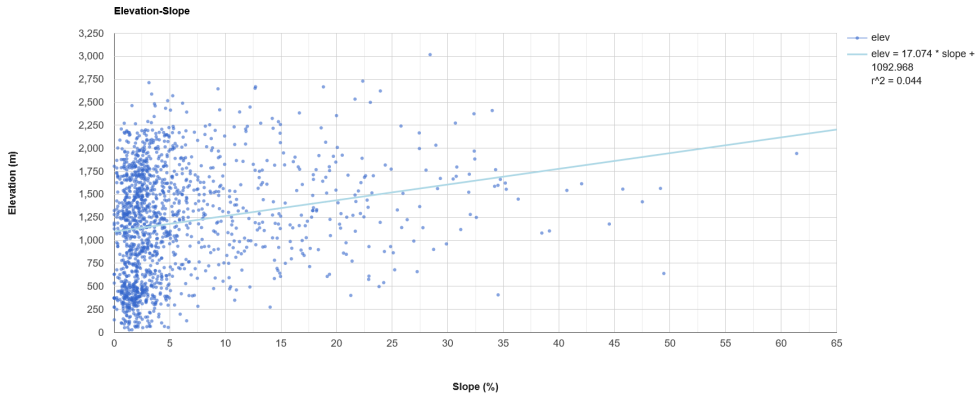
A 6: Linear regression analysis of flood risk (binary) and topographic wetness index (TWI) for 5,000 randomly sampled points across the full study area, encompassing Arizona.



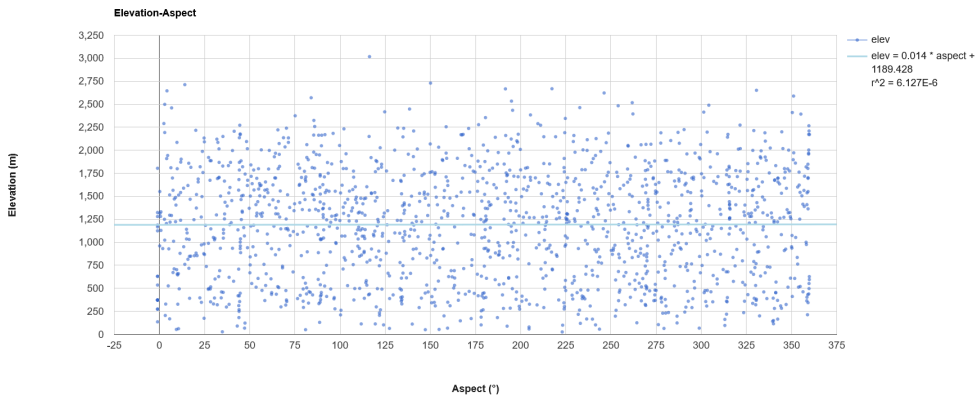
A 7: Linear regression analysis of flood risk (binary) and topographic roughness index (TRI) for 5,000 randomly sampled points across the full study area, encompassing Arizona.



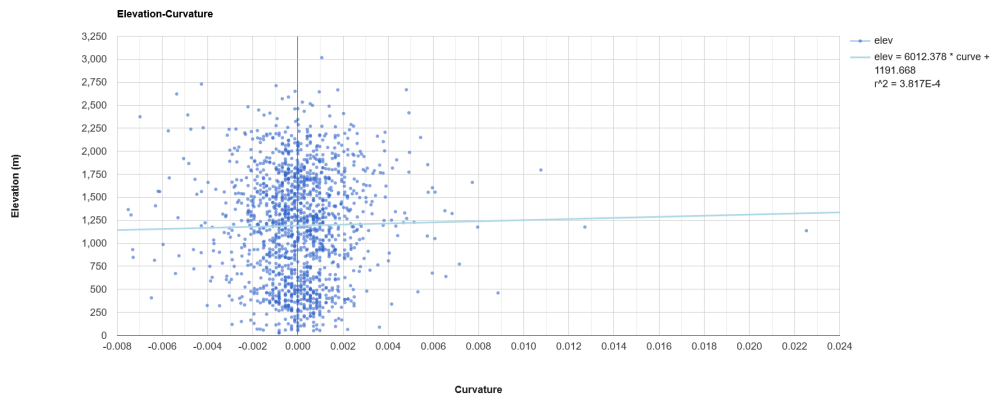
A 8: Linear regression analysis of flood risk (binary) and sediment transport index (STI) for 5,000 randomly sampled points across the full study area, encompassing Arizona.



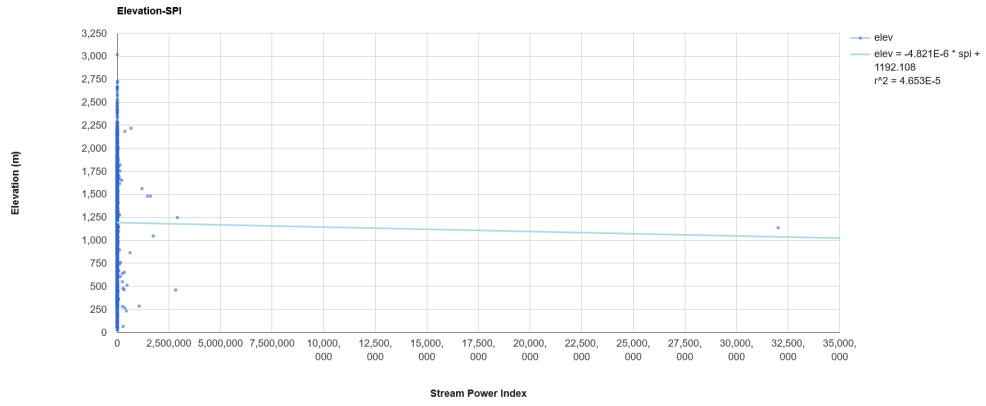
A 9: Linear regression analysis of elevation (m) and slope ($^{\circ}$) for 5,000 randomly sampled points across the full study area, encompassing Arizona.



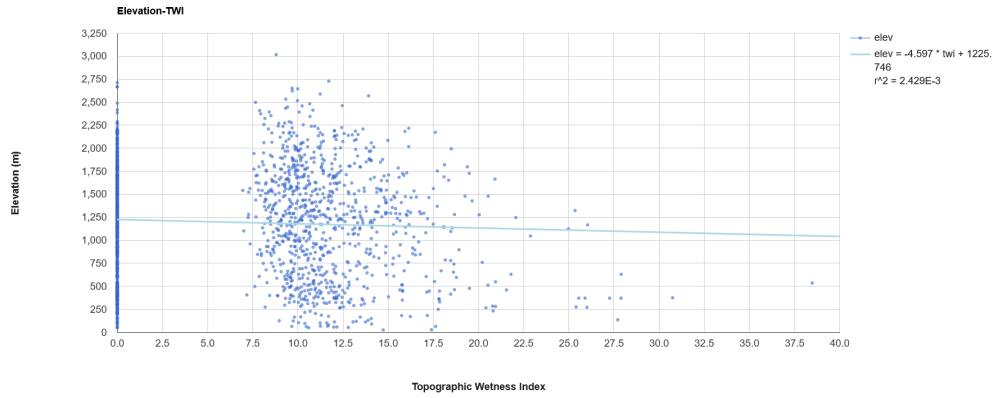
A 10: Linear regression analysis of elevation (m) and aspect ($^{\circ}$) for 5,000 randomly sampled points across the full study area, encompassing Arizona.



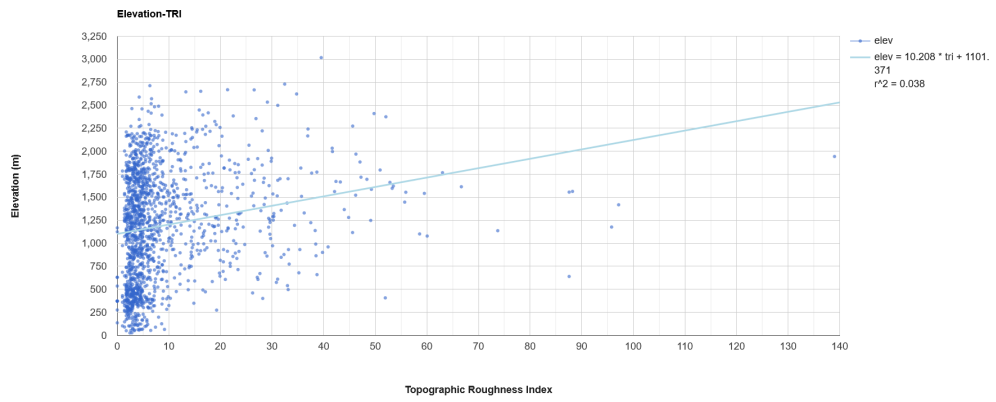
A 11: Linear regression analysis of elevation (m) and curvature for 5,000 randomly sampled points across the full study area, encompassing Arizona.



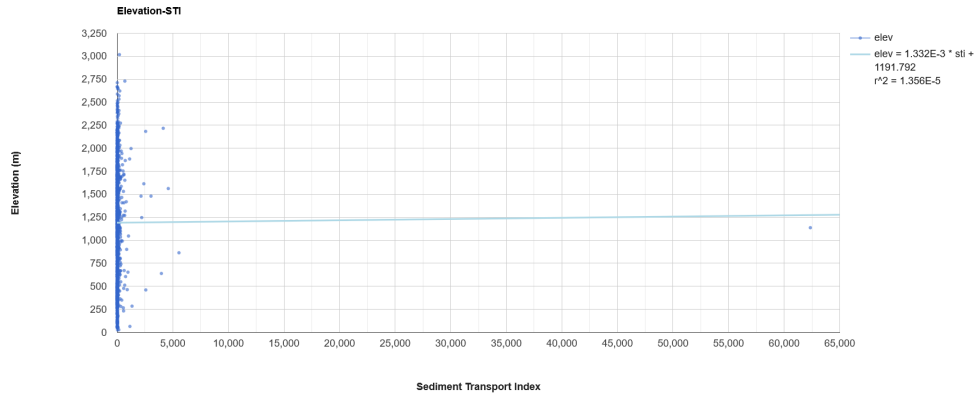
A 12: Linear regression analysis of elevation (m) and stream power index (SPI) for 5,000 randomly sampled points across the full study area, encompassing Arizona.



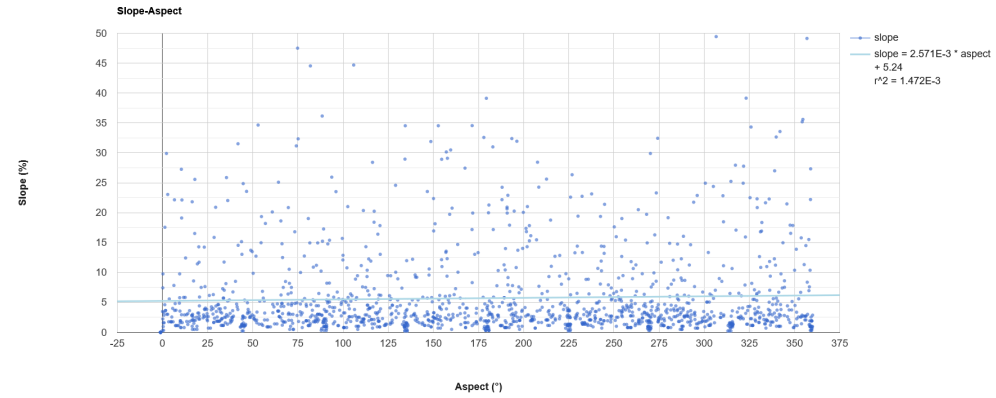
A 13: Linear regression analysis of elevation (m) and topographic wetness index (TWI) for 5,000 randomly sampled points across the full study area, encompassing Arizona.



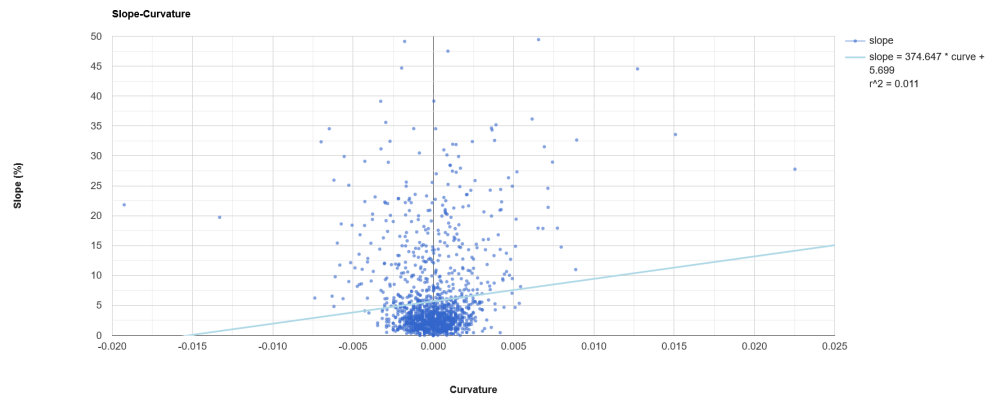
A 14: Linear regression analysis of elevation (m) and topographic roughness index (TRI) for 5,000 randomly sampled points across the full study area, encompassing Arizona.



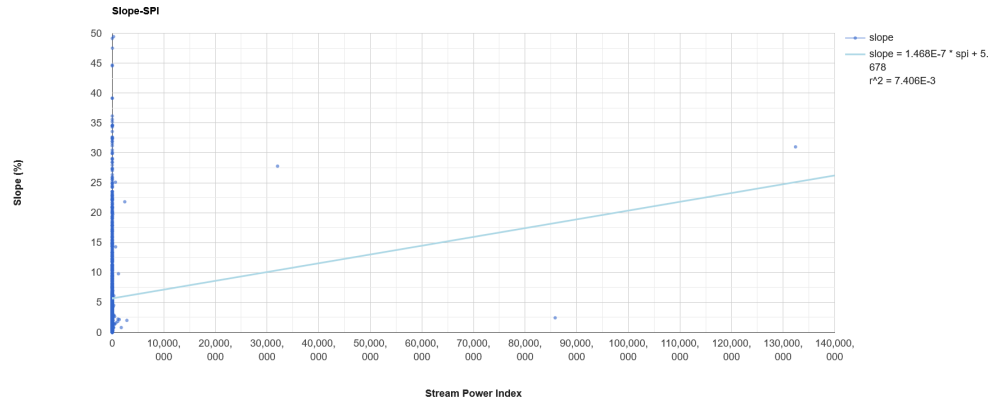
A 15: Linear regression analysis of elevation (m) and sediment transport index (STI) for 5,000 randomly sampled points across the full study area, encompassing Arizona.



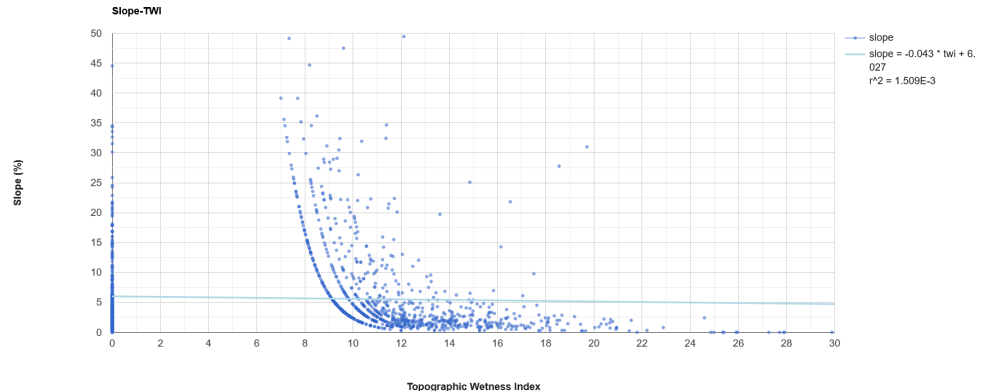
A 16: Linear regression analysis of slope (°) and aspect (°) for 5,000 randomly sampled points across the full study area, encompassing Arizona.



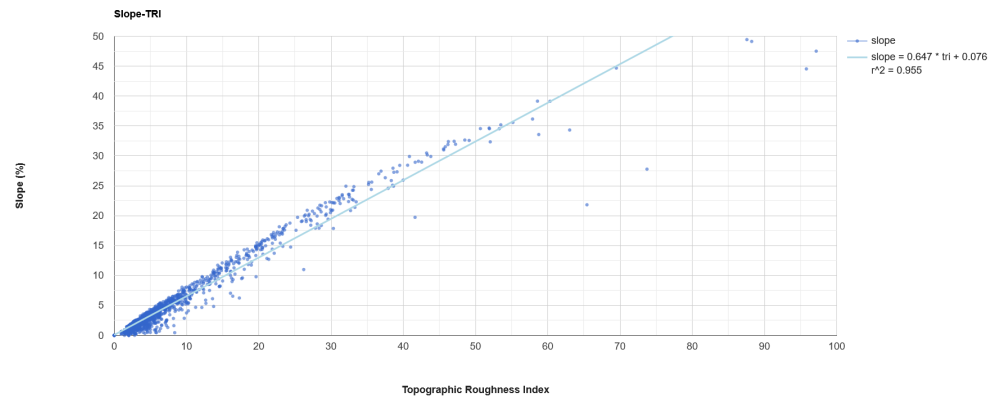
A 17: Linear regression analysis of slope ($^{\circ}$) and curvature for 5,000 randomly sampled points across the full study area, encompassing Arizona.



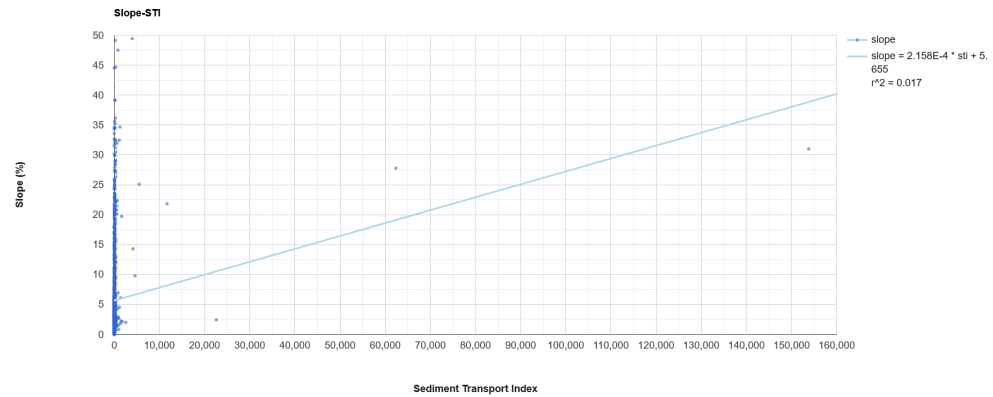
A 18: Linear regression analysis of slope ($^{\circ}$) and stream power index (SPI) for 5,000 randomly sampled points across the full study area, encompassing Arizona.



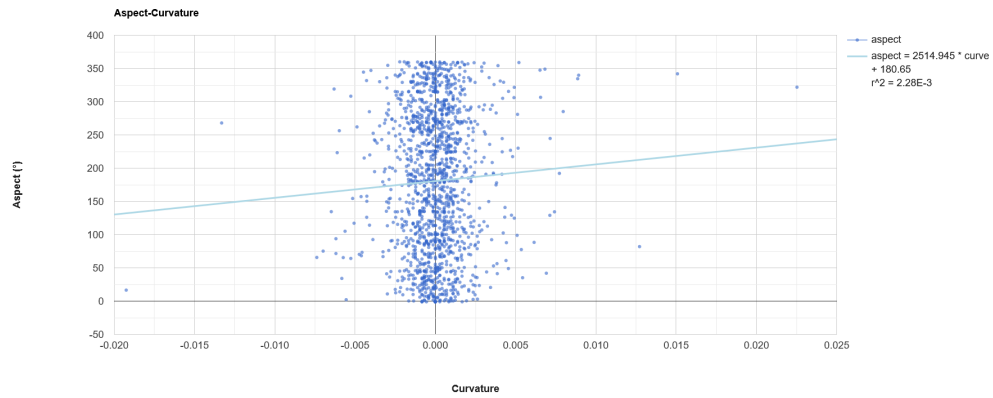
A 19: Linear regression analysis of slope ($^{\circ}$) and topographic wetness index (TWI) for 5,000 randomly sampled points across the full study area, encompassing Arizona.



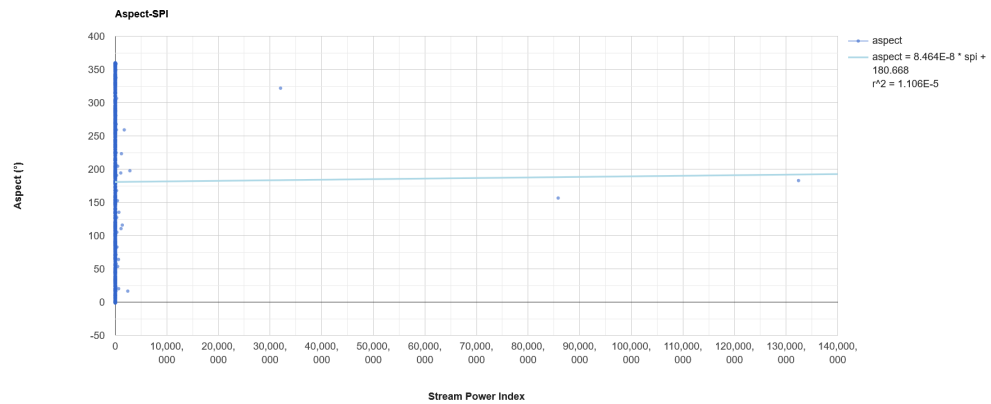
A 20: Linear regression analysis of slope ($^{\circ}$) and topographic roughness index (TRI) for 5,000 randomly sampled points across the full study area, encompassing Arizona.



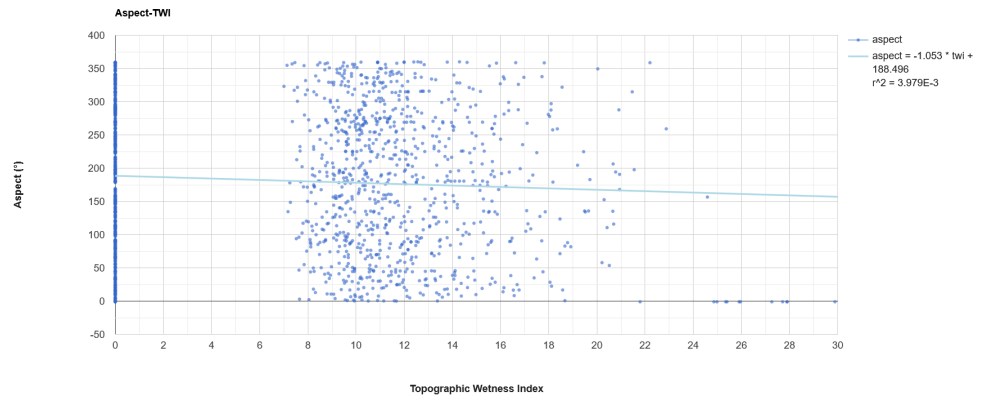
A 21: Linear regression analysis of slope ($^{\circ}$) and sediment transport index (STI) for 5,000 randomly sampled points across the full study area, encompassing Arizona.



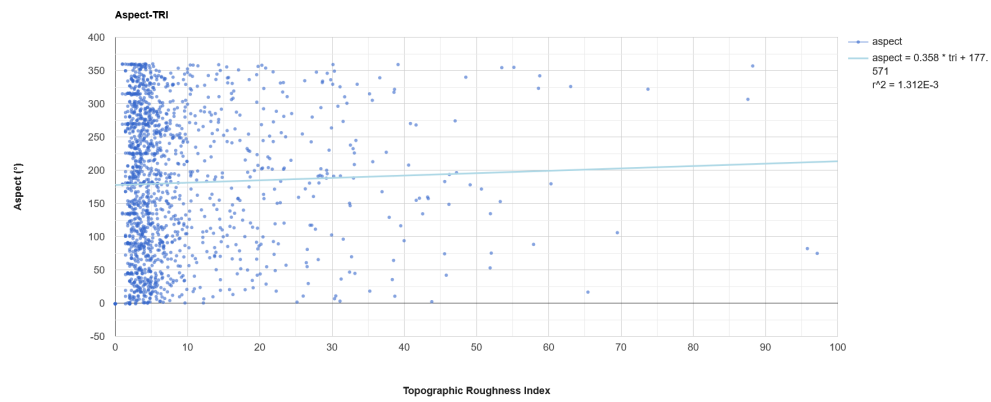
A 22: Linear regression analysis of aspect ($^{\circ}$) and curvature for 5,000 randomly sampled points across the full study area, encompassing Arizona.



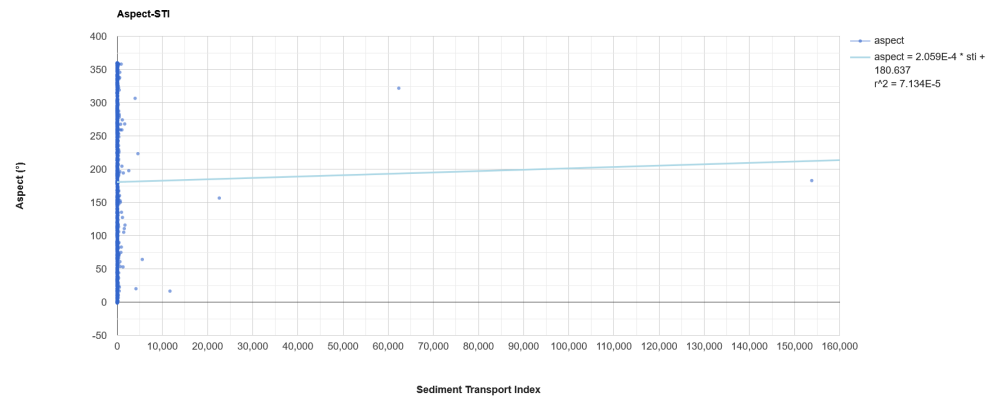
A 23: Linear regression analysis of aspect ($^{\circ}$) and stream power index (SPI) for 5,000 randomly sampled points across the full study area, encompassing Arizona.



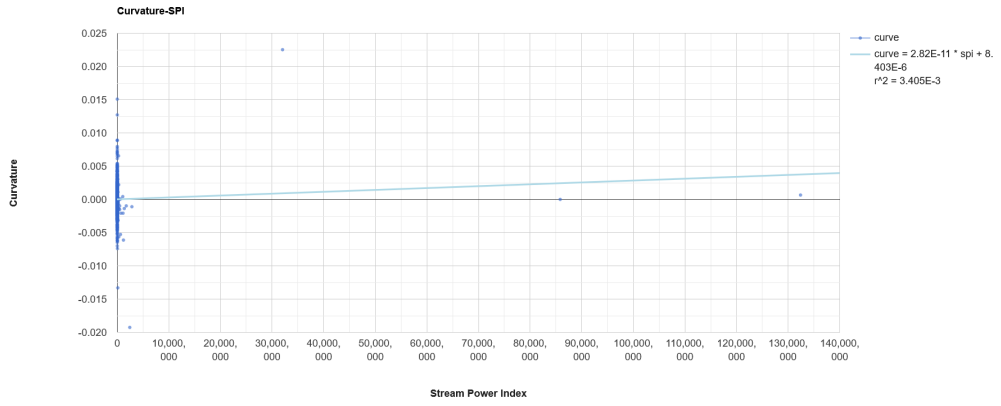
A 24: Linear regression analysis of aspect ($^{\circ}$) and topographic wetness index (TWI) for 5,000 randomly sampled points across the full study area, encompassing Arizona.



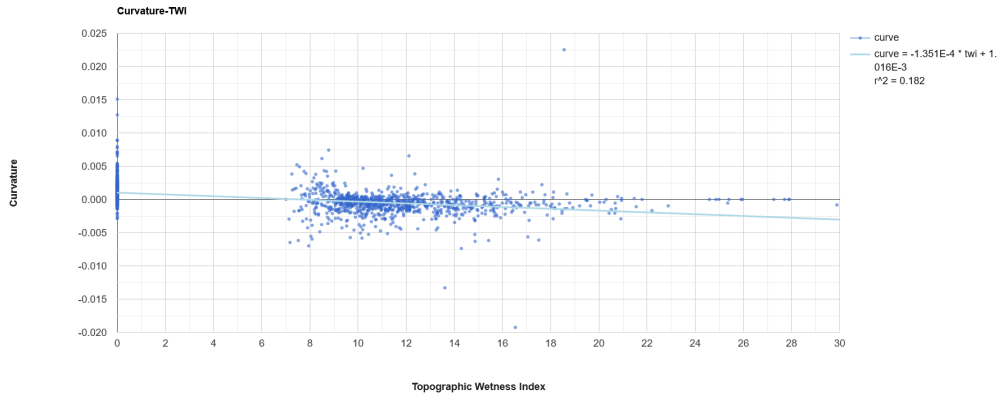
A 25: Linear regression analysis of aspect ($^{\circ}$) and topographic roughness index (TRI) for 5,000 randomly sampled points across the full study area, encompassing Arizona.



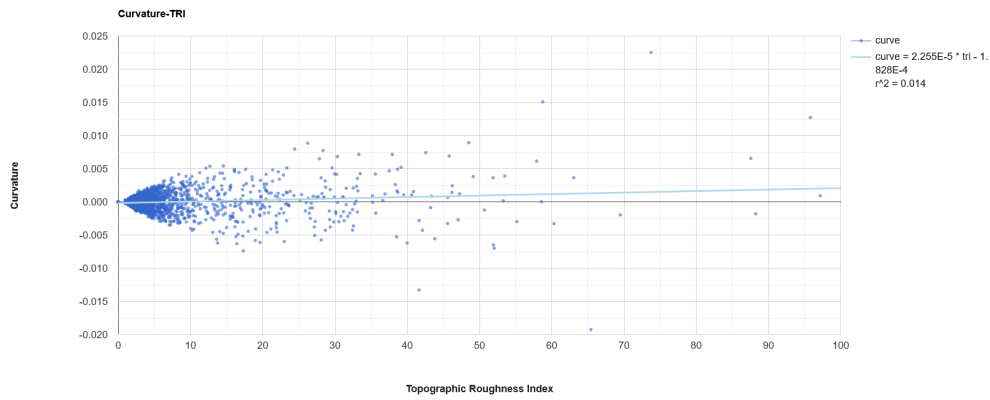
A 26: Linear regression analysis of aspect ($^{\circ}$) and sediment transport index (STI) for 5,000 randomly sampled points across the full study area, encompassing Arizona.



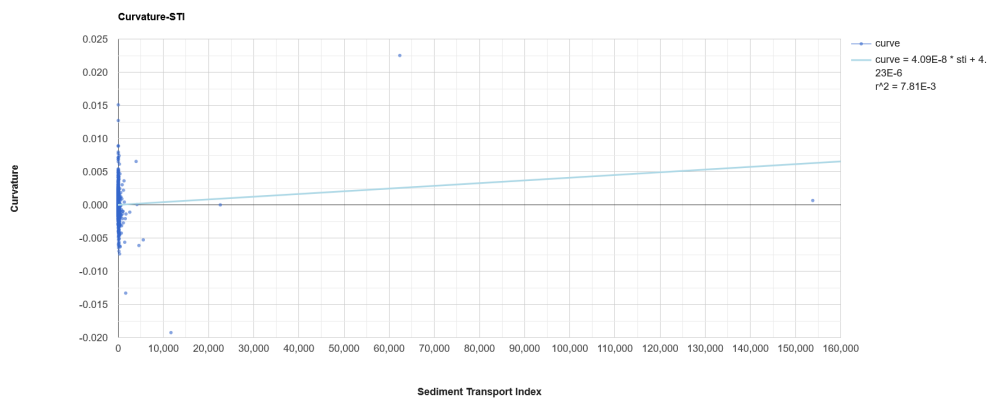
A 27: Linear regression analysis of curvature and stream power index (SPI) for 5,000 randomly sampled points across the full study area, encompassing Arizona.



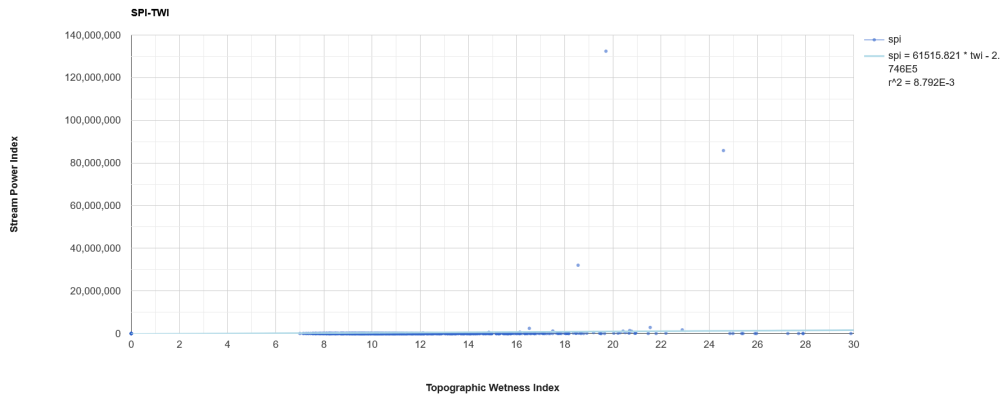
A 28: Linear regression analysis of curvature and topographic wetness index (TWI) for 5,000 randomly sampled points across the full study area, encompassing Arizona.



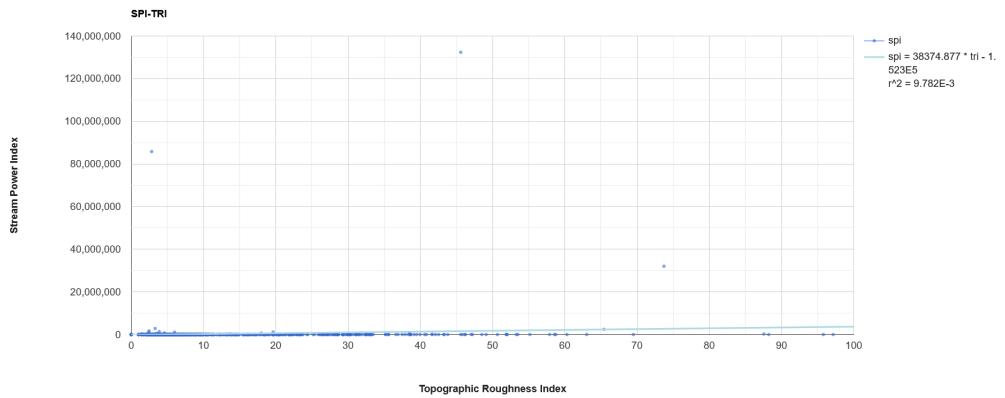
A 29: Linear regression analysis of curvature and topographic roughness index (TRI) for 5,000 randomly sampled points across the full study area, encompassing Arizona.



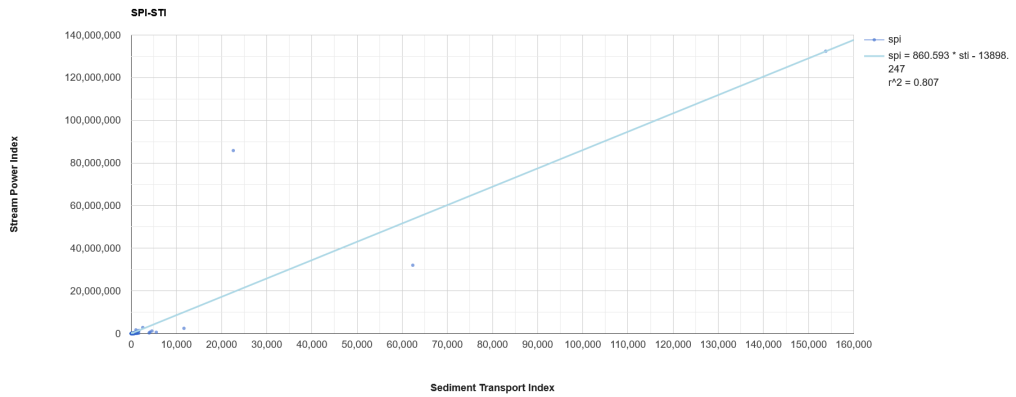
A 30: Linear regression analysis of curvature and sediment transport index (STI) for 5,000 randomly sampled points across the full study area, encompassing Arizona.



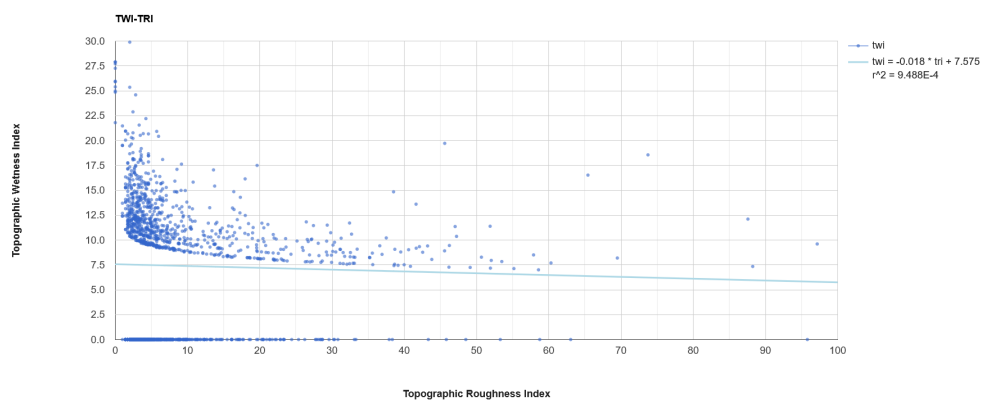
A 31: Linear regression analysis of stream power index (SPI) and topographic wetness index (TWI) for 5,000 randomly sampled points across the full study area, encompassing Arizona.



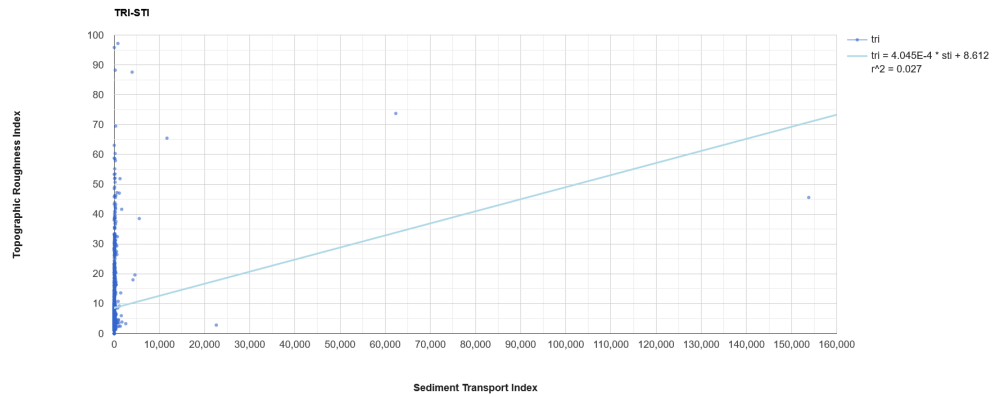
A 32: Linear regression analysis of stream power index (SPI) and topographic roughness index (TRI) for 5,000 randomly sampled points across the full study area, encompassing Arizona.



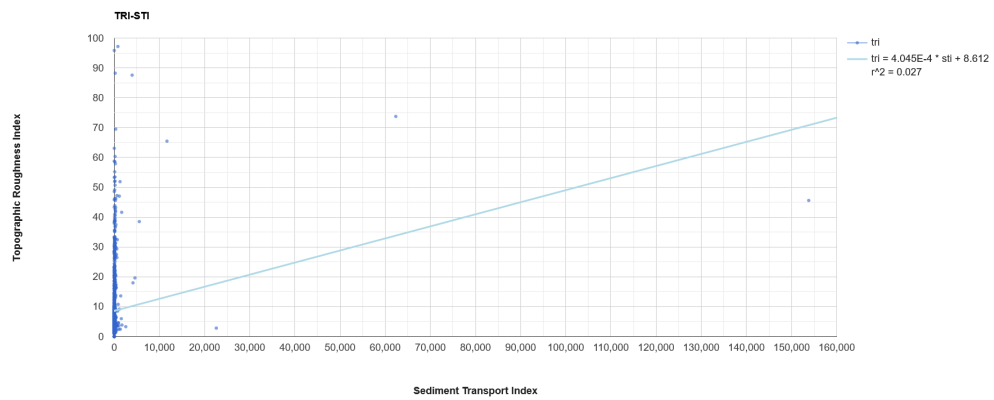
A 33: Linear regression analysis of stream power index (SPI) and sediment transport index (STI) for 5,000 randomly sampled points across the full study area, encompassing Arizona.



A 34: Linear regression analysis of topographic wetness index (TWI) and topographic roughness index (TRI) for 5,000 randomly sampled points across the full study area, encompassing Arizona.



A 35: Linear regression analysis of topographic wetness index (TRI) and sediment transport index (STI) for 5,000 randomly sampled points across the full study area, encompassing Arizona.



A 36: Linear regression analysis of topographic roughness index (TRI) and sediment transport index (STI) for 5,000 randomly sampled points across the full study area, encompassing Arizona.